DNA Nanocages Swallow Gold Nanoparticles (AuNPs) to Form AuNP@DNA Cage Core–Shell Structures

Chuan Zhang,[†] Xiang Li,[†] Cheng Tian,[†] Guimei Yu,[‡] Yulin Li,[†] Wen Jiang,[‡] and Chengde Mao[†,*]

[†]Department of Chemistry and [‡]Markey Center for Structural Biology and Department of Biological Sciences, Purdue University, West Lafayette, Indiana 47907, United States

ABSTRACT DNA offers excellent programming properties to nanomaterials syntheses. Host–guest interaction between DNA nanostructures and inorganic nanoparticles (NPs) is of particular interest because the resulting complexes would possess both programming properties intrinsic to DNA and physical properties associated with inorganic NPs, such as plasmonic and magnetic features. Here, we report a class of core–shell complexes (AuNP@DNA cages): hard gold NPs (AuNPs) are encapsulated in geometrically well-defined soft DNA nanocages. The AuNP guest can be further controllably released from the host (DNA nanocages), pointing to potential applications in surface engineering of inorganic NPs and cargo delivery of DNA nanocages.

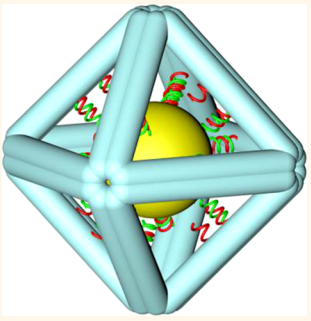

KEYWORDS: DNA nanostructures · self-assembly · nanocages · gold nanoparticles

Host–guest interactions are common phenomena in nature, such as enzyme–substrate interactions.[1] Mimicking this process at the nanoscale is important in nanotechnology, which may facilitate the syntheses of new complex structures that possess properties associated with both the host and guest components. A guest–host pair between gold nanoparticles (AuNPs) and DNA nanocages is of particular interest since AuNPs have many important physical properties in plasmonics, magnetics, and catalysis.[2−5] In the meantime, the self-assembled DNA nanocages which have uniform and tunable sizes and shapes[6−15] have been demonstrated as host scaffolds[14,16] and encapsulating/delivery agents.[12,17−20] When AuNPs are encapsulated in DNA nanocages, the AuNP spherical surfaces are restricted by the host shell (DNA nanocages), providing spatially asymmetric functional sites to the hybrid complexes. In this work, we have developed an encapsulating mechanism (swallowing) for preparation of AuNP@DNA cages, core–shell structures where preassembled DNA nanocages (including DNA tetrahedron, octahedron, and icosahedron) swallow AuNPs into their central cavities to form stable AuNP@DNA nanocage complexes.

AuNP encapsulation is driven by DNA hybridizations between DNA single strands immobilized on AuNPs and single-stranded tails on DNA cages (Figure 1). DNA cages used in this study are a family of symmetric DNA wireframe polyhedra.[21,22] Each of them is assembled from a set of three different DNA strands (colored blue, green, and black-red). The red segments remain as unpaired single-stranded tails in the polyhedra and are located near the middle of the struts. Separately, we functionalize AuNPs with thiolated DNA single strands with sequence complementary to the tails of DNA polyhedra, forming DNA-AuNPs.[23] When incubating the DNA polyhedra and the DNA-AuNPs together, the complementary DNA single strands will hybridize to each other and bring DNA-AuNPs and DNA polyhedra together. Then the DNA-AuNPs will gradually be pulled into the inner volume of the DNA polyhedra to allow more dangling single DNA strands to hybridize. The overall process is like where the DNA cages swallow DNA-AuNPs into their centers.

* Address correspondence to mao@purdue.edu.

Received for review November 22, 2013 and accepted January 12, 2014.

Published online January 13, 2014
10.1021/nn406039p

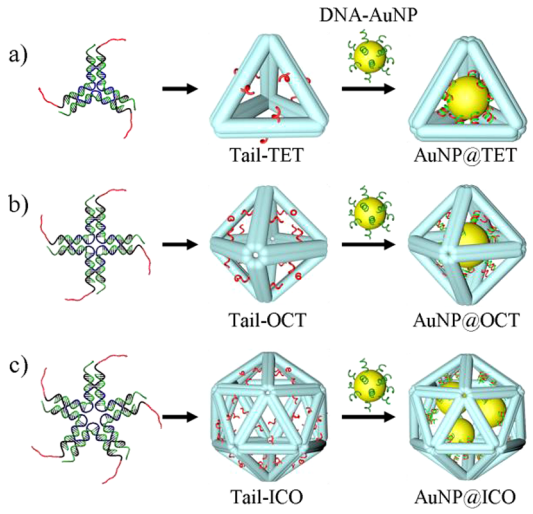

Figure 1. DNA polyhedra encapsulate gold nanoparticles (AuNPs) to form core−shell structures (AuNP@cages). Star-shaped nanomotifs[21,22] assemble into symmetric DNA polyhedra: tetrahedron (TET), octahedron (OCT), and icosahedron (ICO). Two unpaired, single-stranded tails (red) are dangling on each strut. When incubating with DNA-AuNPs (solid yellow spheres) that are AuNPs functionalized with complementary DNA single strands (bright green), the DNA-AuNPs will be swallowed into the tail-polyhedra driven by maximization of DNA hybridization between the single-stranded tails (red) on DNA polyhedra and the DNA single strands (green) immobilized on DNA-AuNPs. The number of guest AuNPs that will be swallowed by a DNA cage depends on the inner volume of the DNA cage.

The number of DNA-AuNPs being swallowed will be determined by the size of the DNA cages.

RESULTS AND DISCUSSION

DNA nanocages with single-stranded tails were assembled from three types of unique strands: a long, repetitive, blue strand (Ln; $n = 3-5$), a medium green strand (M), and a short, peripheral, black-red strand (S).[21,22] The assembly is a simple, one-pot process: the corresponding DNA strands (Ln/M/S = 1:n:n) were mixed in a Mg^{2+}-containing, neutral, aqueous buffer and slowly cooled from 95 to 25 °C over 48 h. Upon formation, the DNA nanocages were directly analyzed by polyacrylamide gel electrophoresis (PAGE, Supporting Information Figure S1). All designed tail-polyhedra formed well and appeared as sharp bands with expected electrophoretic mobilities when compared to previously characterized DNA polyhedra (without single-stranded tails).[21,22]

AuNP encapsulation was conducted by simply incubating the tailed DNA polyhedra with single DNA strand-functionalized AuNPs (DNA-AuNPs) at room temperature overnight. The AuNP size was chosen by two factors: (i) The inner volume of the DNA polyhedra. In the current design, all edges of the DNA polyhedra have the same length (~14 nm). The diameters of the largest spheres that can be held inside are 7.9, 12.0, and 20.6 nm for DNA-TET, OCT, and ICO, respectively. (ii) The pore size of the DNA polyhedra. All DNA

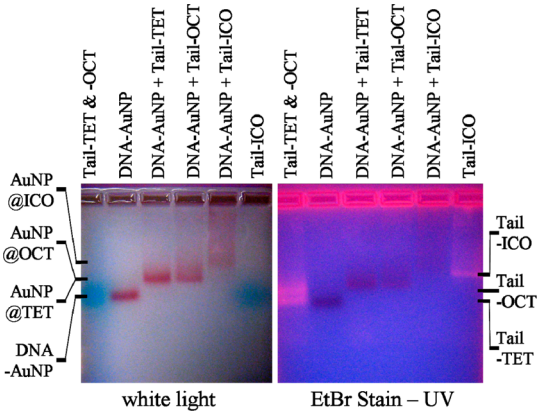

Figure 2. Agarose gel (2%) electrophoretical analysis of the AuNP@cage formation. The sample composition in each lane and the identity of each band are indicated above and beside the gel images, respectively. The two images are from the same gel. The left image is taken under white light illumination to show the AuNP-containing species as AuNPs are red-purple. Note that DNA is not visible under such a condition. The two blue bands are due to tracking dyes used for monitoring the electrophoresis. The right image is taken with UV illumination after the gel is stained with ethidium bromide (EtBr). After EtBr staining, DNA shows red-orange fluorescence under UV light. Note the EtBr fluorescence will be quenched by AuNPs in AuNP-containing species (which appear as dark bands).

polyhedra in this study have triangular faces. The largest spherical particle that can pass the triangular pore without destroying the DNA polyhedra is 6.1 nm in diameter. Hence a 5 nm AuNP (commercially available) was chosen for the current study. After being functionalized with single-stranded DNA, the overall DNA-AuNP size would increase because of the soft, deformable DNA corona.

Upon hybridization between DNA tails on polyhedra and single strands on DNA-AuNPs, AuNPs were encapsulated into the DNA polyhedra, resulting in the formation of AuNP@TET, AuNP@OCT, and AuNP@ICO complexes. The encapsulation was first monitored by agarose gel electrophoresis (Figure 2). Compared to original mobilities of either DNA nanocages or individual DNA-AuNPs, the AuNP@cage complexes had much lower mobility because of their higher molecular weights. In the cases of TET (with 12 tails) and OCT (with 24 tails) encapsulations, a major single band appeared on the gel when equal ratio of the cages/AuNPs was used (counting on the particles). Though both AuNPs and tail-polyhedra had multiple single strands, they formed 1:1 complexes between AuNPs and DNA polyhedra and no serious cross-linking happened. We reasoned that, at low concentration, when the first pair of their complementary single strands (on a DNA-AuNP and a polyhedron separately) recognized and bound to each other, all other strands would be brought into proximity with each other and facilitated their hybridization. As the process proceeded, the AuNPs would go into the center of the polyhedron to maximize the DNA hybridization and lower the free energy of the system. Thus, the free energy (ΔG) was negative for the favorable

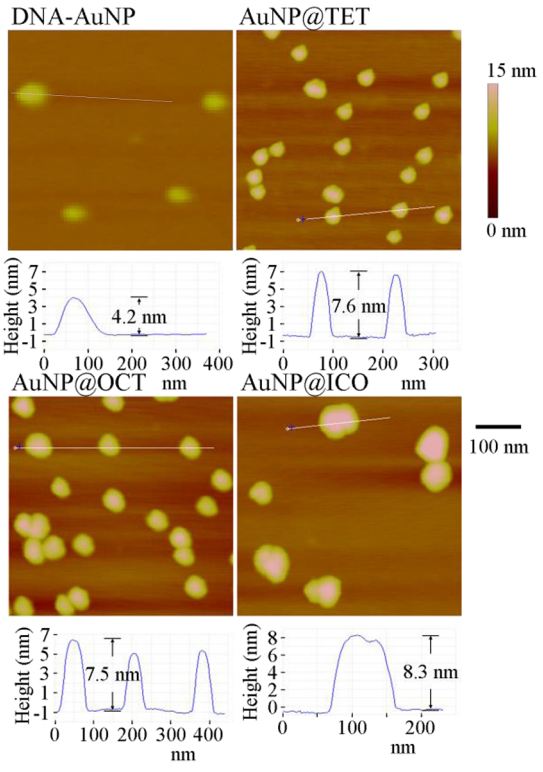

Figure 3. AFM characterization of AuNP@cage complexes. All images have the same scale bars as shown on the right. For each sample, a section analysis is shown below the corresponding AFM image.

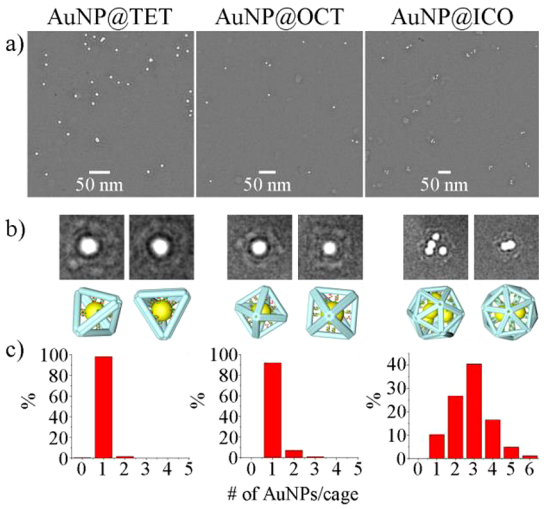

Figure 4. Cryogenic electron microscopy (cryoEM) study of the AuNP@cage complexes. (a) Raw cryoEM images of AuNP@cage complexes. AuNPs have very strong contrast in cryoEM and appear as white spots. (b) (Top panel) Representative single particle complexes from raw images and (bottom panel) corresponding structural models at similar orientations. In the zoom-in images, the DNA cages (with much lower contrast) are visible surrounding the bright AuNPs. (c) Distributions of the numbers of AuNPs encapsulated in each DNA cage. For each case, 500 complexes have been counted.

encapsulation process even though the swallowing was associated with the entropy decreasing since more ordered structures formed. To facilitate the swallowing process and the formation of AuNP@cage core−shell structures, the effect of ΔG decrease should be a dominate factor over the entropy decrease. Once inside the polyhedron, the AuNP could not reach another DNA polyhedron anymore, thus preventing cross-linking (Figure S2; with varied ratios, excess AuNPs remain as free particles on the gel). However, the encapsulation of AuNPs by DNA-ICO (with 120 tails) behaved differently. The AuNP@ICO smeared in the gel when excess AuNPs were added, indicating mixture complexes formed. The inner cavity of DNA-ICO was large enough to hold a 20.6 nm sphere, far larger than the 5 nm AuNP. So each icosahedron could host multiple AuNPs.

The AuNP@nanocage complexes were further characterized by atomic force microscope (AFM, Figure 3 and Figure S3) and dynamic light scattering (DLS) technique (Figure S4). AFM imaging showed that both AuNP@TET and AuNP@OCT complexes were quite uniform in size. The particles were significantly taller than free DNA-AuNPs (~5 nm). During the AFM imaging (in air), dehydration and strong DNA−substrate interaction would collapse the DNA cages. The dried DNA frames sandwiched the AuNPs, resulting in heights taller than that of DNA-AuNP. The AuNP@ICO complex was less uniform than AuNP@TET and AuNP@OCT complexes under AFM imaging. The section analysis on a representative particle gave shoulder peaks, indicating that the complex contains two or more AuNPs. It was consistent with electrophoresis data. Both gel and AFM imaging demonstrated that the tail-ICO could host multiple AuNPs inside. The conclusion was further confirmed by DLS study (Figure S4), which directly measured the hydrodynamic diameters of the complexes. Before encapsulation, both DNA-AuNPs and the DNA polyhedra gave reasonable diameters with quite narrow distributions. After encapsulation, the AuNP@cage complexes show slightly increased diameter (3−5 nm) compared with the corresponding tail-polyhedra. We suspected that such increases in apparent hydrodynamic diameters were not due to the real size expansion but the dramatic increase of molecular weight of the objects. After incorporating AuNPs, the Brownian motion of the hybrid complexes in a solution would decrease; hence the apparent hydrodynamic diameters slightly shifted to a larger number.

Finally, we applied cryogenic electron microscopy (cryoEM) to study the AuNP@cage complexes (Figure 4). A very thin layer of AuNP@cage complex-containing solution was quickly frozen and directly imaged. This protocol avoided dehydration-induced complex denaturation and artifacts. Under low dose of electron beam, both AuNPs and DNA frameworks could be observed at the same time. In the raw images of AuNP@TET and AuNP@OCT samples, the bright 5 nm AuNPs (strong EM signal) were

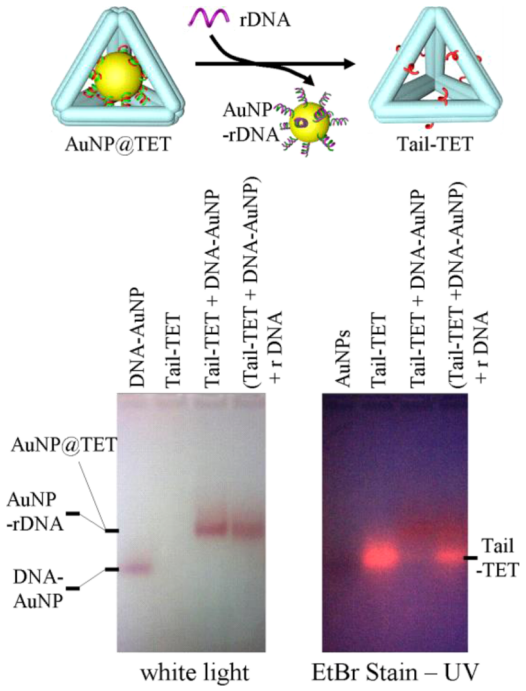

Figure 5. Release of AuNPs from the DNA nanocages. Release strand (rDNA) is complementary to the DNA immobilized on AuNPs and can displace the single-stranded tails of TET and release AuNPs from tail-TET. In the right image, note the disappearance of the tail-TET after incubation of DNA-AuNPs and the regeneration of the free tail-TET after addition of rDNA.

surrounded by a dim DNA framework (weak EM signal). The visible DNA frameworks still kept their original tetrahedral or octahedral shapes at the expected sizes. The raw object images were consistent with the 2D projections of structural models (Figure 4b). The edges of DNA frames were ~14 nm long, matching the designed DNA polyhedra (13.8 nm), assuming a rise of 0.33 nm/base pair and a diameter of 2 nm for a DNA duplex. Almost no free AuNPs or empty TET and OCT were observed. Over 90% of the objects were 1:1 AuNP−polyhedron complexes. Cross-linking between two complexes was very rare. Consistent with studies of electrophoresis and AFM imaging, the ICO behaved differently and could encapsulate multiple (1−6) AuNPs. CryoEM imaging allowed direct counting of the number of AuNPs hosted in each ICO. We noticed that encapsulation of multiple AuNPs caused deformation of many ICOs, presumably due to breaking the symmetry of the ICOs and that the large ICO was easier to deform than the small TET and OCT.

The AuNPs could be released, as well (Figure 5). When adding an excess amount of DNA single strands (release DNA or rDNA) with sequence fully complementary to the DNA strands on the DNA-AuNPs, they could hybridize with the DNA strands on DNA-AuNPs and displace the DNA tails of the DNA cages.[24,25] Thus, the interaction between DNA-AuNPs and DNA cages would be diminished, and DNA-AuNPs would be released from the nanocages, resulting in the original, empty DNA polyhedra and free DNA duplex-modified AuNPs. AuNP@TET complex had been used to demonstrate this concept. Note that the released DNA-AuNPs were coated with DNA duplexes instead of original single strands; thus the released duplex DNA-coated AuNPs migrated much slower than the original single-stranded DNA-coated AuNP but similar to the AuNP@TET.

CONCLUSIONS

In summary, we have successfully demonstrated that self-assembled DNA polyhedra can encapsulate AuNPs into their interior spaces through a swallow mechanism. The resulting hybrid AuNP@cage structures have significant potentials in nanotechnology and materials science. The DNA polyhedral frames break the spherical symmetry of the spherical AuNPs and introduce the programmability of DNA onto AuNPs. We envision that once deliberate interactions are further introduced on DNA frames, such AuNP@cage complexes will behave like atoms with defined valence and bonding direction for assembly of molecule-like AuNP architectures.[26] We also believe that a similar strategy can be applied to other inorganic particles, such as quantum dots[27,28] and magnetic nanoparticles,[29] which forges the syntheses of new materials with specific and predesigned functions. We are currently actively pursuing those opportunities.[30]

MATERIALS AND METHODS

Oligonucleotides. DNA sequences were adapted from previous works, which were originally designed by a computer program "SEQUIN" [Seeman, N. C. De novo design of sequences for nucleic-acid structural engineering. *J. Biomol. Struct. Dyn.* **1990**, *8*, 573−581]. All oligonucleotides were purchased from IDT, Inc. and purified by 10−20% denaturing polyacrylamide gel electrophoresis (PAGE).

DNA sequences for DNA polyhedron self-assembly:

L3: 5′-Agg CAC CAT CgT Agg TTT TTC TTg CCA ggC ACC ATC gTA ggT TTT TCT TgC CAg gCA CCA TCg TAg gTT TTT CTT gCC-3′.

L4: 5′-Agg CAC CAT CgT Agg TTT TTC TTg CCA ggC ACC ATC gTA ggT TTT TCT TgC CAg gCA CCA TCg Tag gTT TTT CTTg CCA ggC ACC ATC gTA ggT TTT TCT TgC C-3′

L5: 5′-Agg CAC CAT CgT Agg TTT TTC TTg CCA ggC ACC ATC gTA ggT TTT TCT TgC CAg gCA CCA TCg Tag gTT TTT CTT gCC Agg CAC CAT CgT Agg TTT TTC TTg CCA ggC ACC ATC gTA ggT TTT TCT TgC C-3′

M: 5′-AgC AAC CTg CCT ggC AAg CCT ACg ATg gAC ACg gTA ACg ACT-3′.

S: 5′-ACC gTg Tgg TTg CTA gTC gTT TT CCT CAA gA-3′ (tail sequence is underlined).

Thiol-DNA: 5′-TCT TgA ggT TTT TTT TTT-SH-3′

rDNA: 5′-AAA AAA CCT CAA gA-3′.

LS: 5′-Tgg TgC CTg gCA AgA A-3′

For the central strands **L4** and **L5**, the purchased strands were first purified by 10−15% PAGE gel in denaturing condition. Then the purified strand was phosphorylated by T4 polynucleotide kinase (New England Biolabs, Inc.) under 37 °C for 2 h. Finally 4- or 5-fold of linker strand (Strand LS) was added in the phosphorylated product and followed with ~3 μL of T4 DNA ligase (New England Biolabs, Inc.) addition. The mixed solution

was incubated overnight at room temperature. After phenol extraction to remove the protein, the ligated circularized central strand was purified from the mixture by 10% PAGE gel and ready to use.

AuNPs were purchased from Ted Pella.

Formation of Tail-TET, -OCT, and -ICO. DNA strands L, M, and S mixed in TAE/Mg^{2+} buffer, which contained 40 mM Tris base (pH 8.0), 20 mM acetic acid, 2 mM EDTA, and 12.5 mM magnesium acetate. Then the mixtures were heated up to 95 °C and slowly cooled to room temperature (~25 °C) in 48 h. Then the assembled DNA tail-polyhedra were ready to use for characterizations and AuNP encapsulation.

Tail-TET: L3 + M + S (70:210:210 nM)
Tail-OCT: L4 + M + S (50:200:200 nM)
Tail-ICO: L5 + M + S (30:150:150 nM)

AuNP Modification. First the thiol-DNA strand was incubated with 100 mM DTT solution in PBS buffer (137 mM NaCl, 12 mM phosphate, 2.7 mM KCl, pH 7.4). After 30 min, the salt and excessive DTT were removed by size-exclusion chromatography with a Sephadex G25 column (GE Healthcare). Then the DNA solution was added to citrate-capped AuNP solution with a ratio of 100 strands per particle and incubated for 30 min. Then, stepwise additions of 5.0 M NaCl (with each aliquot raising the total NaCl concentration by approximately 0.05 M) were added to the solution at 1 h intervals. Once a final salt concentration of 0.5 M sodium chloride was reached, the solution was further incubated overnight to allow for maximum DNA loading. The resulting DNA-AuNPs were then purified with multiple rounds of centrifuging the nanoparticles down and removing the supernatant.

AuNP Encapsulation and Release. In order to encapsulate DNA-AuNPs into the DNA tail-polyhedra, DNA-AuNP and tail-polyhedron with ratios in a range of 2:1 to 1:2 were mixed together in TAE/Mg^{2+} buffer. Then the mixtures were incubated overnight at room temperature (25 °C). The concentration of tail-polyhedra and DNA-AuNPs was determined by the UV−vis measurement at 260 or 520 nm using the extinction coefficients obtained from the companies. To release the AuNPs from the tail-DNA TET, 2-fold excess rDNA was added into the AuNP@TET sample and the mixture was further incubated overnight at 37 °C.

Gel Electrophoresis. Nondenaturing gels were used to check the formation of DNA polyhedra with tails. The gels containing 2.5% polyacrylamide (19:1 acrylamide/bisacrylamide) were run on an FB-VE10-1 electrophoresis unit (FisherBiotech) at 4 °C (80 V, constant voltage). The running buffer was TAE/Mg^{2+} buffer. Before electrophoresis, the DNA samples were concentrated with Microcon YM-50 (cutoff molecular weight: 50 kDa) centrifugal filter units to ~200 nM counting the motifs. After electrophoresis, the gels were stained with Stains-All (Sigma) and scanned. The encapsulation and release of the AuNPs were monitored by agarose gel electrophoresis, where 2% w/v agarose was dissolved in TAE/Mg^{2+} buffer and the gel was run on an FB-SB-710 electrophoresis unit (FisherBiotech) at 4 °C (50 V, constant voltage). The gels were stained with ethidium bromide (Sigma) and photographed under both white light and UV illumination (302 nm).

AFM Imaging. A drop of 1.5 μL sample solution was spotted onto freshly cleaved mica surface (Ted Pella, Inc.) and incubated for 10 s to allow the sample to absorb onto the substrate. The sample drop was then washed off by 30 μL of 2 mM magnesium acetate solution and dried by compressed air. DNA samples were imaged in air in tapping mode on a Multimode AFM with Nanoscope IIIa controller (Veeco) using oxide-sharpened silicon probes having a resonance frequency in the range of 280−340 kHz (MikroMasch-NSC15). The tip−surface interaction was minimized by optimizing the scan set point to the highest possible value. AFM imaging was performed at 25 °C.

Dynamic Light Scattering (DLS) Measurement. The DLS measurements were performed with 100 μL DNA sample solutions on Malvern Zetasizer Nano-ZS (Malvern Instruments, UK) with light wavelength of 633 nm. Five parallel measurements were tested.

CryoEM Imaging. The AuNP@cage solutions were first concentrated by Amicon Ultra centrifugal filter (Ultracel-100k Membrane, Millipore Ltd.) to a final DNA concentration of ~1−2 μM (in terms of complex structures). A drop of 3 μL of concentrated sample solution was pipetted onto glow discharged Quantifoil hole grid (Electron Microscopy Sciences, QUANTIFOILR 2/2) and then blotted by filter paper and immediately plunge-frozen into ethane slush cooled by liquid nitrogen on an FEI Vitrobot system. The images were taken on FEI CM200 TEM with accelerating voltage of 200 kV. The optimized condition with a low-dose exposure (~20 e/Å^2) was used to minimize radiation damage to the samples and vitreous ice. Contrast of DNA frames was enhanced by taking the image under focuses in the range of 2−4 μm, recorded by Kodak films. The calibrated magnification was 51 040×, resulting in a pixel size of 1.25 Å.

Conflict of Interest: The authors declare no competing financial interest.

Acknowledgment. We thank ONR and NSF for supporting this work.

Supporting Information Available: Additional figures as described in the text (Figure S1−S4) are available. This material is available free of charge *via* the Internet at http://pubs.acs.org.

REFERENCES AND NOTES

1. Glasner, M. E.; Gerlt, J. A.; Babbitt, P. C. Evolution of Enzyme Superfamilies. *Curr. Opin. Chem. Biol.* **2006**, *10*, 492–497.
2. Daniel, M. C.; Astruc, D. Gold Nanoparticles: Assembly, Supramolecular Chemistry, Quantum-Size-Related Properties, and Applications toward Biology, Catalysis, and Nanotechnology. *Chem. Rev.* **2004**, *104*, 293–346.
3. Hu, M.; Chen, J.; Li, Z.; Au, L.; Hartland, G. V.; Li, X.; Marquez, M.; Xia, Y. Gold Nanostructures: Engineering Their Plasmonic Properties for Biomedical Applications. *Chem. Soc. Rev.* **2006**, *35*, 1084–1094.
4. Crespo, P.; Litrán, R.; Rojas, T. C.; Multigner, M.; de la Fuente, J. M.; Sánchez-López, J. C.; García, M. A.; Hernando, A.; Penadés, S.; Fernández, A. Permanent Magnetism, Magnetic Anisotropy, and Hysteresis of Thiol-Capped Gold Nanoparticles. *Phys. Rev. Lett.* **2004**, *93*, 087204–087207.
5. Corma, A.; Garcia, H. Supported Gold Nanoparticles as Catalysts for Organic Reactions. *Chem. Soc. Rev.* **2008**, *37*, 2096–2126.
6. Chen, J. H.; Seeman, N. C. Synthesis from DNA of a Molecule with the Connectivity of a Cube. *Nature* **1991**, *350*, 631–633.
7. Zhang, Y. W.; Seeman, N. C. Construction of A DNA-Truncated Octahedron. *J. Am. Chem. Soc.* **1994**, *116*, 1661–1669.
8. Shih, W. M.; Quispe, J. D.; Joyce, G. F. A 1.7-kilobase Single-Stranded DNA That Folds into a Nanoscale Octahedron. *Nature* **2004**, *427*, 618–621.
9. Goodman, R. P.; Schaap, I. A. T.; Tardin, C. F.; Erben, C. M.; Berry, R. M.; Schmidt, C. F.; Turberfield, A. J. Rapid Chiral Assembly of Rigid DNA Building Blocks for Molecular Nanofabrication. *Science* **2005**, *310*, 1661–1665.
10. Rothemund, P. W. K. Folding DNA To Create Nanoscale Shapes and Patterns. *Nature* **2006**, *440*, 297–302.
11. Bhatia, D.; Mehtab, S.; Drishnan, R.; Indi, S. S.; Basu, A.; Krishnan, Y. Icosahedral DNA Nanocapsules by Modular Assembly. *Angew. Chem., Int. Ed.* **2009**, *48*, 4134–4137.
12. Andersen, E. S.; Dong, M.; Nielsen, M. M.; Jahn, K.; Subramani, R.; Mamdouh, W.; Golas, M. M.; Sander, B.; Stark, H.; Oliveira, C. L. P.; *et al.* Self-Assembly of a Nanoscale DNA Box with a Controllable Lid. *Nature* **2009**, *459*, 73–76.
13. Douglas, S. M.; Dietz, H.; Liedl, T.; Högberg, B.; Graf, F.; Shih, W. M. Self-Assembly of DNA into Nanoscale Three-Dimensional Shapes. *Nature* **2009**, *459*, 414–418.
14. Ke, Y. G.; Sharma, J.; Liu, M.; Jahn, K.; Liu, Y.; Yan, H. Scaffolded DNA Origami of a DNA Tetrahedron Molecular Container. *Nano Lett.* **2009**, *9*, 2445–2447.
15. Zhang, C.; He, Y.; Su, M.; Ko, S. H.; Ye, T.; Leng, Y.; Sun, X.; Ribbe, A. E.; Jiang, W.; Mao, C. DNA Self-Assembly: From 2D to 3D. *Faraday Discuss.* **2009**, *143*, 221–233.

16. Pal, S.; Deng, Z. T.; Ding, B. Q.; Yan, H.; Liu, Y. DNA-Origami-Directed Self-Assembly of Discrete Silver-Nanoparticle Architectures. *Angew. Chem., Int. Ed.* **2010**, *49*, 2700–2704.
17. Zhao, Z.; Jacovetty, E. L.; Liu, Y.; Yan, H. Encapsulation of Gold Nanoparticles in a DNA Origami Cage. *Angew. Chem., Int. Ed.* **2011**, *50*, 2041–2044.
18. Lo, P. K.; Karam, P.; Aldaye, F. A.; McLaughlin, C. K.; Hamblin, G. D.; Cosa, G.; Sleiman, H. F. Loading and Selective Release of Cargo in DNA Nanotubes with Longitudinal Variation. *Nat. Chem.* **2010**, *2*, 319–328.
19. Erben, C. M.; Goodman, R. P.; Turberfield, A. J. Single-Molecule Protein Encapsulation in a Rigid DNA Cage. *Angew. Chem., Int. Ed.* **2006**, *45*, 7414–7417.
20. Douglas, S. M.; Bachelet, I.; Church, G. M. A Logic-Gated Nanorobot for Targeted Transport of Molecular Payloads. *Science* **2012**, *335*, 831–834.
21. He, Y.; Ye, T.; Su, M.; Zhang, C.; Ribbe, A. E.; Jiang, W.; Mao, C. Hierarchical Self-Assembly of DNA into Symmetric Supramolecular Polyhedra. *Nature* **2008**, *452*, 198–201.
22. Zhang, C.; Su, M.; He, Y.; Zhao, X.; Fang, P.; Ribbe, A. E.; Jiang, W.; Mao, C. Conformational Flexibility Facilitates Self-Assembly of Complex DNA Nanostructures. *Proc. Natl. Acad. Sci. U.S.A.* **2008**, *105*, 10665–10669.
23. Mirkin, C. A.; Letsinger, R. L.; Mucic, R. C.; Storhoff, J. J. A DNA-Based Method for Rationally Assembling Nanoparticles into Macroscopic Materials. *Nature* **1996**, *382*, 607–609.
24. Yurke, B.; Turberfield, A. J.; Mills, A. P.; Simmel, F. C.; Neumann, J. L. A DNA-Fuelled Molecular Machine Made of DNA. *Nature* **2000**, *406*, 605–608.
25. Zhang, D. Y.; Seelig, G. Dynamic DNA Nanotechnology Using Strand-Displacement Reactions. *Nat. Chem.* **2011**, *3*, 103–113.
26. Mastroianni, A.; Claridge, S.; Alivisatos, A. P. Pyramidal and Chiral Groupings of Gold Nanocrystals Assembled Using DNA Scaffolds. *J. Am. Chem. Soc.* **2009**, *131*, 8455–8459.
27. Tikhomirov, G.; Hoogland, S.; Lee, P. E.; Fischer, A.; Sargent, E. H.; Kelley, S. O. DNA-Based Programming of Quantum Dot Valency, Self-Assembly and Luminescence. *Nat. Nanotechnol.* **2011**, *6*, 485–490.
28. Samanta, A.; Deng, Z.; Liu, Y.; Yan, H. A Perspective on Functionalizing Colloidal Quantum Dots with DNA. *Nano Res.* **2013**, *6*, 853–870.
29. Zhang, C.; Macfarlane, R. J.; Young, K. L.; Choi, C. H. J.; Hao, L.; Auyeung, E.; Liu, G.; Zhou, X.; Mirkin, C. A. A General Approach to DNA-Programmable Atom Equivalents. *Nat. Mater.* **2013**, *12*, 741–746.
30. Licata, N. A.; TKachenko, A. V. Self-Assembling DNA-caged Particles: Nanoblocks for Hierarchical Self-Assembly. *Phy. Rev. E.* **2009**, *79*, 011404.